

$pp \rightarrow ppK^+K^-$ reaction at high energies

P. Lebiedowicz^{1,*} and A. Szczurek^{2,1,†}

¹*Institute of Nuclear Physics PAN, PL-31-342 Cracow, Poland*

²*University of Rzeszów, PL-35-959 Rzeszów, Poland*

Abstract

We evaluate differential distributions for the four-body $pp \rightarrow ppK^+K^-$ reaction at high energies which constitutes an irreducible background to three-body processes $pp \rightarrow ppM$, where $M = \phi, f_2(1275), f'_2(1525), f_0(1500), \chi_{c0}$. We consider central diffractive contribution mediated by Pomeron and Reggeon exchanges as well as completely new mechanism of emission of kaons from the proton lines. We include absorption effects due to proton-proton interaction and kaon-kaon rescattering. We compare our results with measured cross sections for the CERN ISR experiment. We make predictions for future experiments at RHIC, Tevatron and LHC. Differential distributions in invariant two-kaon mass, kaon rapidities and transverse momenta of kaons are presented. The two-dimensional distribution in (y_{K^+}, y_{K^-}) is particularly interesting. The higher the incident energy, the higher preference for the same-hemisphere emission of kaons. We find that the kaons from the new mechanism of emission directly from proton lines are produced rather forward and backward but the corresponding cross section is rather small. The processes considered here constitute a sizeable contribution to the total proton-proton cross section as well as to kaon inclusive cross section.

We consider a measurement of exclusive production of scalar χ_{c0} meson in the proton-proton collisions via $\chi_{c0} \rightarrow K^+K^-$ decay. The corresponding amplitude for exclusive central diffractive χ_{c0} meson production was obtained within the k_t -factorization approach including virtualities of active gluons and the corresponding cross section is calculated with the help of unintegrated gluon distribution functions (UGDFs) known from the literature. The influence of kinematical cuts on the signal-to-background ratio is investigated. Corresponding experimental consequences are discussed.

Keywords: Diffractive processes, KK continuum, $\chi_c(0^+) \rightarrow K^+K^-$ decay

PACS numbers: 13.87.Ce, 13.60.Le, 13.85.Lg

*Electronic address: piotr.lebiedowicz@ifj.edu.pl

†Electronic address: antoni.szczurek@ifj.edu.pl

I. INTRODUCTION

The exclusive $pp \rightarrow ppK^+K^-$ reaction was studied only at low energy [1, 2]. Here the dominant mechanisms are exclusive $a_0(980)$ and $f_0(980)$ production [1] or excitation of nucleon and Λ resonances [2]. The main aim of this paper is to discuss mechanisms of exclusive K^+K^- production in hadron-hadron collisions at high energies. Processes of central exclusive production became recently a very active field of research (see e.g. Ref. [3] and references therein). Although the attention is paid mainly to high- p_t processes that can be used for new physics searches (exclusive Higgs, $\gamma\gamma$ interactions, etc.), measurements of low- p_t signals are also very important as they can help to constrain models of the backgrounds for the former ones. The $pp \rightarrow ppK^+K^-$ reaction is a natural background for exclusive production of resonances decaying into K^+K^- channel, such as: ϕ , $f_2(1270)$, $f_2'(1525)$, $f_0(1500)$, χ_{c0} . The expected non-resonant background can be modeled using a "non-perturbative" framework, mediated by Pomeron-Pomeron fusion with an intermediate off-shell pion/kaon exchanged between the final-state particle pairs. The two-pion background to exclusive production of $f_0(1500)$ meson was discussed in Ref. [4]. In Refs.[5, 6] we have studied production of $\pi^+\pi^-$ pairs for low and high energies. Here we wish to present similar analysis for K^+K^- production at high energies. The dominant mechanism of the $pp \rightarrow pp\pi^+\pi^-$, $pp \rightarrow ppK^+K^-$ reactions at high energies is relatively simple compared to that of the $pp \rightarrow nn\pi^+\pi^+$ [7] or $pp \rightarrow pp\pi^0\pi^0$ processes. In Ref. [8] a possible measurement of the exclusive $\pi^+\pi^-$ production at the LHC with tagged forward protons has been studied.

The recent works (Refs. [9–13] and references therein) concentrated on the production of χ_c mesons where the QCD mechanism is similar to the exclusive production of the Higgs boson. Furthermore, the $\chi_{c(0,2)}$ states are expected to annihilate via two-gluon processes into light mesons and may, therefore, allow study of glueball production dynamics [14].

Recently, the CDF Collaboration has measured the cross section for central exclusive production of χ_c mesons in proton-antiproton collisions at the Tevatron [15], by selecting events with large rapidity gaps separating the centrally produced state from the dissociation products of the incoming protons. In this experiment χ_c mesons are identified via decay to the $J/\psi + \gamma$ with $J/\psi \rightarrow \mu^+\mu^-$ channel. At the Tevatron the experimental invariant mass resolution was not sufficient to distinguish between scalar, axial and tensor χ_c . While the branching fractions to this channel for axial and tensor mesons are large [16] ($\mathcal{B} = (34.4 \pm 1.5)\%$ and $\mathcal{B} = (19.5 \pm 0.8)\%$, respectively) the branching fraction for the scalar meson is very small $\mathcal{B} = (1.16 \pm 0.08)\%$ [16]. On the other hand, the cross section for exclusive χ_{c0} production obtained within the k_t -factorization is much bigger than that for χ_{c1} and χ_{c2} . As a consequence, all χ_c mesons give similar contributions [11] to the $J/\psi + \gamma$ decay channel. Clearly, the measurement via decay to the $J/\psi + \gamma$ channel cannot provide cross section for different χ_c .

The scalar χ_{c0} meson decays into several two-body channels (e.g. $\pi\pi$, K^+K^- , $p\bar{p}$) or four-body hadronic modes (e.g. $\pi^+\pi^-\pi^+\pi^-$, $\pi^+\pi^-K^+K^-$). The observation of χ_{c0} CEP via two-body decay channels is of special interest for studying the dynamics of heavy quarkonia. The measurement of exclusive production of χ_{c0} meson in proton-(anti)proton collisions via $\chi_{c0} \rightarrow \pi^+\pi^-$ decay has been already discussed in Ref. [17]. In the present paper we analyze a possibility to measure χ_{c0} via its decay to K^+K^- channel. The branching fraction to this channel is relatively large $\mathcal{B}(\chi_{c0} \rightarrow K^+K^-) = (0.61 \pm 0.035)\%$ [16]. In addition, the axial χ_{c1} does not decay to the KK channel and the branching ratio for the χ_{c2} decay into two kaons is smaller $\mathcal{B}(\chi_{c2} \rightarrow K^+K^-) = (0.109 \pm 0.008)\%$ [16]. A much smaller cross section for

χ_{c2} production means, in practice, that only χ_{c0} will contribute to the signal.

Exclusive charmonium decays have been a subject of interest at the e^+e^- colliders as they are an excellent laboratory for studying quark-gluon dynamics at relatively low energies. Thus, a measurement of many exclusive hadronic χ_{cJ} decays if possible is very valuable. Although these χ_{cJ} states are not directly produced in e^+e^- collisions, they are copiously produced in the radiative decays $\psi(2S) \rightarrow \gamma\chi_{cJ}$, each of which has a branching ratio of around 9% [16]. Recently the BESIII Collaboration performed a measurement of the hadronic decays of the three χ_{cJ} states to $p\bar{p}K^+K^-$ ($\bar{p}K^+\Lambda(1520)$, $\Lambda(1520)\bar{\Lambda}(1520)$ and $\phi p\bar{p}$) [18]. In the present paper we discuss a possibility to measure the different decay channels in proton-(anti)proton collisions in order to determine the cross section for exclusive production of the P-wave charmonia. Here, continuum backgrounds are expected to be larger than in the e^+e^- collisions and this requires a separate discussion. We will discuss this issue in the present paper.

II. CENTRAL DIFFRACTIVE CONTRIBUTION

A. The KN scattering

In order to fix parameters of our double Pomeron exchange (DPE) model we consider first elastic KN scattering. The forward amplitudes $M_{KN}(s, t=0)$ of the elastic scatterings are written in terms of the Regge exchanges

$$\begin{aligned} M_{K^\pm p \rightarrow K^\pm p}(s, 0) &= A_P(s, 0) + A_{f_2}(s, 0) + A_{a_2}(s, 0) \mp A_\omega(s, 0) \mp A_\rho(s, 0), \\ M_{K^\pm n \rightarrow K^\pm n}(s, 0) &= A_P(s, 0) + A_{f_2}(s, 0) - A_{a_2}(s, 0) \mp A_\omega(s, 0) \pm A_\rho(s, 0). \end{aligned} \quad (2.1)$$

The optical theorem relates the total cross section for the scattering of a pair of hadrons to the amplitude for elastic scattering: $\text{Im}M_{el}(s, t=0) \sim s\sigma_{tot}(s)$. When the centre-of-mass energy \sqrt{s} is large the elastic KN scattering amplitude is a sum of the terms:

$$A_i(s, t) = \eta_i s C_i^{KN} \left(\frac{s}{s_0} \right)^{\alpha_i(t)-1} \exp \left(\frac{B_{KN}^i}{2} t \right), \quad (2.2)$$

where $i = P, f_2, a_2, \omega$ and ρ . The energy scale s_0 is fixed at $s_0 = 1 \text{ GeV}^2$. The values of coupling constants (C_i^{KN}) are taken from the Donnachie-Landshoff analysis of the total cross section in several hadronic reactions [19]. The parameters of Regge linear trajectories ($\alpha_i(t) = \alpha_i(0) + \alpha'_i t$) and signature factors (η_i) used in the present calculations are listed in Table I. The slope of the elastic KN scattering can be written as

$$B(s) = B_{KN}^i + 2\alpha'_i \ln \left(\frac{s}{s_0} \right) \quad (2.3)$$

and only the B_{KN}^i parameters are adjusted to the existing experimental data for the elastic KN scattering.

The differential elastic cross section is expressed with the help of the elastic scattering amplitude as usually:

$$\frac{d\sigma_{el}}{dt} = \frac{1}{16\pi s^2} |M_{KN}(s, t)|^2. \quad (2.4)$$

The differential distributions $d\sigma_{el}/dt$ for both K^+p and K^-p elastic scattering for three incident-beam momenta of $P_{lab} = 5$ GeV, $P_{lab} = 50$ GeV and $P_{lab} = 200$ GeV are shown in Fig.1. With the slope pareamters, as in Ref. [6], $B_P^{KN} = B_P^{\pi N} = 5.5 \text{ GeV}^{-2}$, $B_R^{KN} = B_R^{\pi N} = 4 \text{ GeV}^{-2}$ for Pomeron and Reggeon exchanges, a rather good description of experimental $d\sigma_{el}/dt$ is achieved. The exception is the low energy K^+p scattering. Here Λ baryon exchange is a possible mechanism in addition to Pomeron and Reggeon exchanges.

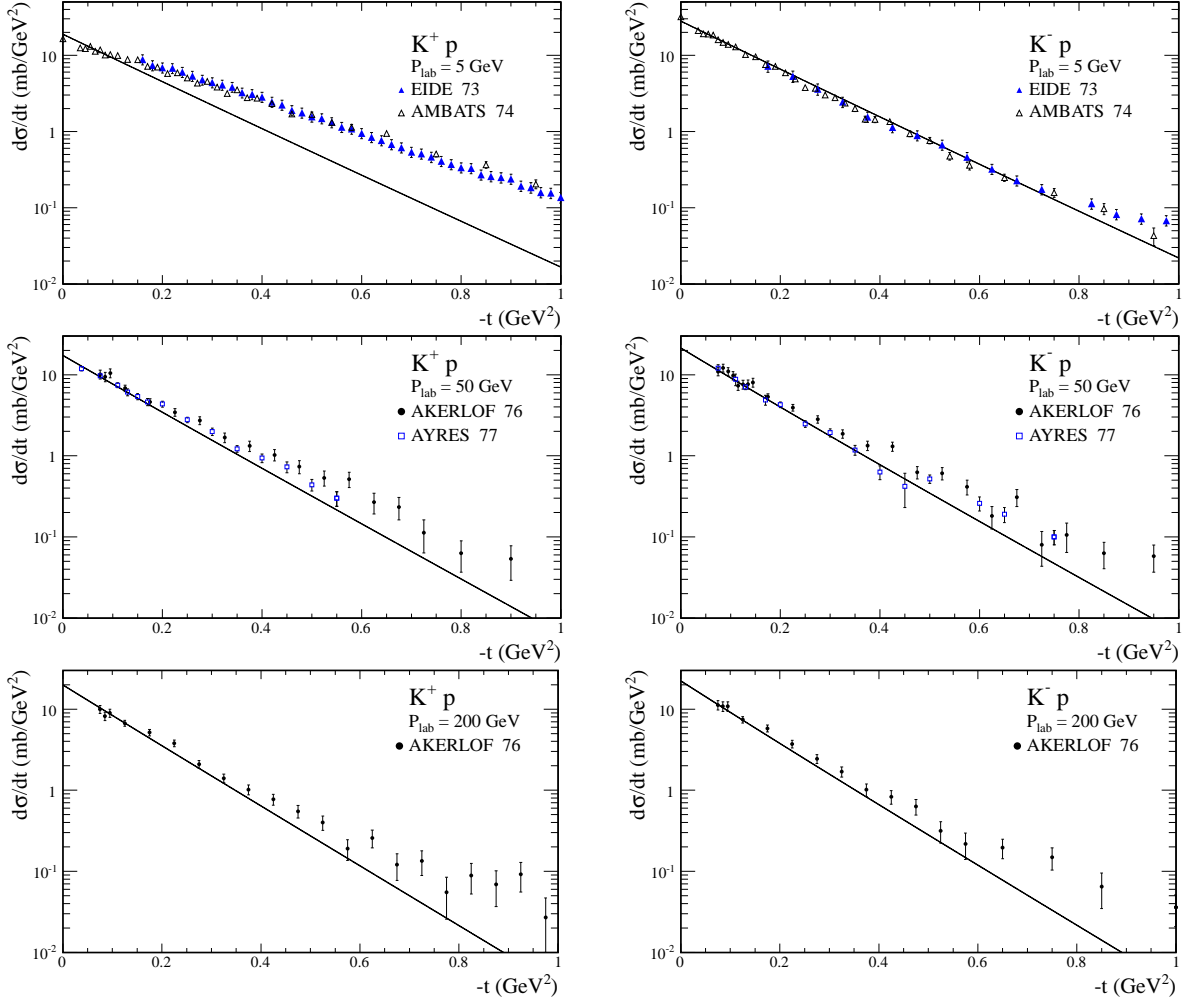


FIG. 1: Differential distributions for K^+p (left) and K^-p (right) elastic scattering for three incident-beam momenta of $P_{lab} = 5, 50, 200$ GeV. The experimental data are taken from Refs [20].

We nicely describe the existing experimental data for elastic KN scattering for $\sqrt{s} > 3$ GeV. as can be seen from Fig.2. In the Regge approach, high energy cross section is dominated by Pomeron exchange (dashed lines). The Reggeon exchanges dominate in the resonance region (dash-dotted lines). While the total cross section is just a sum of the Pomeron and Reggeon terms, the elastic cross section have the interference term (long-dashed lines). In order to exclude low energy regions the $M_{KN}(s, t)$ elastic scattering amplitudes are corrected by purely phenomenological smooth cut-off correction factor (as in Ref. [6]).

Our model sufficiently well describes the KN data and includes absorption effects due to kaon-nucleon rescatterings in an effective way. This has a clear advantage for applications

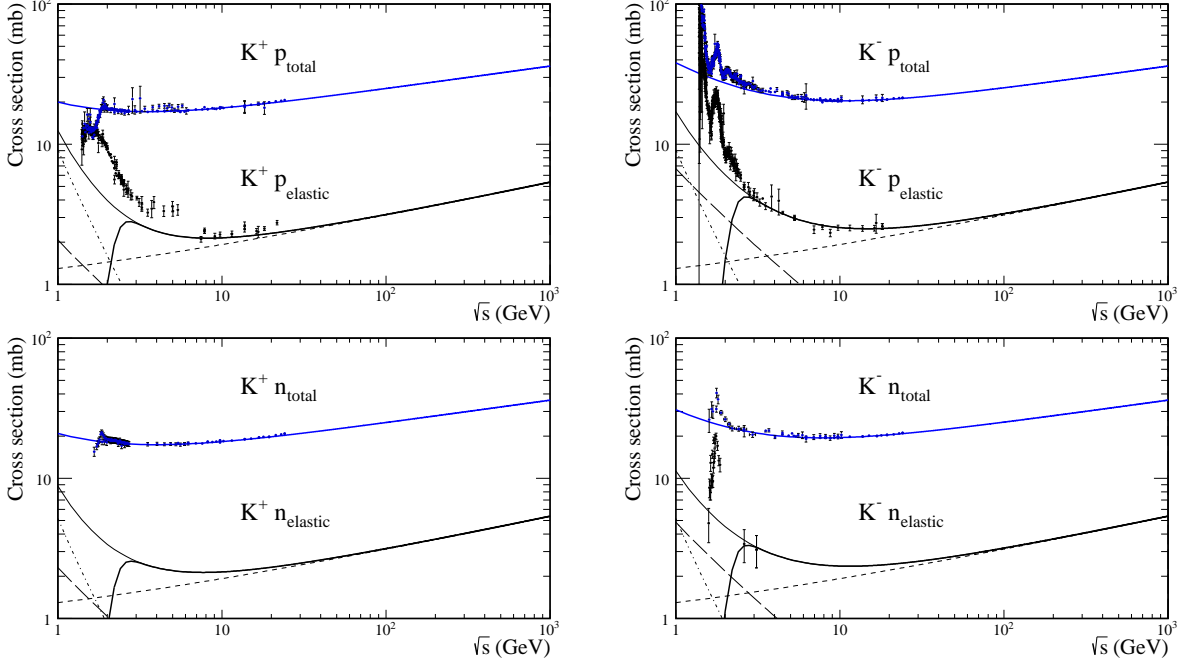


FIG. 2: The integrated cross section for the KN total and elastic scattering. The experimental data are taken from particle data book [16]. The lines are explained in the main text.

TABLE I: Parameters of Pomeron and Reggeon exchanges determined from elastic and total cross sections used in the present calculations.

i	η_i	$\alpha_i(t)$	C_i^{NN} (mb)	C_i^{KN} (mb)	C_i^{KK} (mb)
\mathbb{P}	i	$1.0808 + (0.25 \text{ GeV}^{-2}) t$	21.7	11.82	$\simeq 6.438$
f_2	$(-0.860895 + i)$	$0.5475 + (0.93 \text{ GeV}^{-2}) t$	75.4875	15.67	$\simeq 3.253$
ρ	$(-1.16158 - i)$	$0.5475 + (0.93 \text{ GeV}^{-2}) t$	1.0925	2.05	$\simeq 3.847$
a_2	$(-0.860895 + i)$	$0.5475 + (0.93 \text{ GeV}^{-2}) t$	1.7475	1.585	$\simeq 1.438$
ω	$(-1.16158 - i)$	$0.5475 + (0.93 \text{ GeV}^{-2}) t$	20.0625	7.055	$\simeq 2.481$

to the $pp \rightarrow ppK^+K^-$ reaction where the KN absorption effects do not need to be included explicitly. Having fixed the parameters we can proceed to our four-body $pp \rightarrow ppK^+K^-$ reaction.

B. Central diffractive production of K^+K^-

The dominant mechanism of the exclusive production of K^+K^- pairs at high energies is sketched in Fig. 3. The formalism used in the calculation of the amplitude is explained in detail elsewhere for the $\pi^+\pi^-$ production [6, 17] and here only main aspects are discussed. The full amplitude for the process $pp \rightarrow pK^+K^-p$ (with four-momenta $p_a + p_b \rightarrow p_1 + p_3 + p_4 + p_2$, respectively) is a sum of the Born and rescattering amplitudes

$$\mathcal{M}_{pp \rightarrow ppKK}^{full} = \mathcal{M}^{Born} + \mathcal{M}^{pp-rescatt.} + \mathcal{M}^{KK-rescatt.}. \quad (2.5)$$

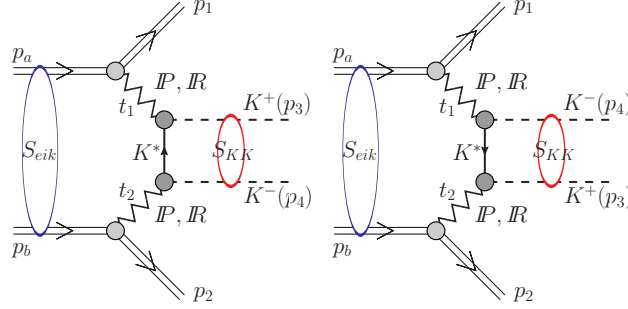


FIG. 3: The central diffractive mechanism of exclusive production of K^+K^- pairs including the absorptive corrections due to proton-proton interactions as well as kaon-kaon rescattering.

The Born amplitude can be written as

$$\begin{aligned} \mathcal{M}^{Born} = & M_{13}(s_{13}, t_1) F_K(\hat{t}) \frac{1}{\hat{t} - m_K^2} F_K(\hat{t}) M_{24}(s_{24}, t_2) \\ & + M_{14}(s_{14}, t_1) F_K(\hat{u}) \frac{1}{\hat{u} - m_K^2} F_K(\hat{u}) M_{23}(s_{23}, t_2), \end{aligned} \quad (2.6)$$

where $M_{ik}(s_{ik}, t_i)$ denotes "interaction" between forward proton ($i = 1$) or backward proton ($i = 2$) and one of the two kaons ($k = 3$ for K^+ , $k = 4$ for K^-). The energy dependence of the KN elastic amplitudes is parameterized in terms of Pomeron and f_2 , a_2 , ω and ρ Reggeon exchanges as explained in section II A. The Donnachie-Landshoff parametrization is used only above resonance regions for the KN subsystem energy $\sqrt{s_{ik}} > 2 - 3$ GeV. In order to exclude resonance regions the M_{ik} terms are corrected by a purely phenomenological smooth cut-off correction factors which in practice modify the cross section only at large rapidities [6].

The kaon exchange as a meson exchange is a correct description at rather low energies. At higher energies a kaon reggeization is required [17]. This is done by the following replacement:

$$\frac{1}{\hat{t}/\hat{u} - m_K^2} \rightarrow \beta_M(\hat{s}) \frac{1}{\hat{t}/\hat{u} - m_K^2} + \beta_R(\hat{s}) \mathcal{P}^K(\hat{t}/\hat{u}, \hat{s}), \quad (2.7)$$

where we have introduced the kaon Regge propagator $\mathcal{P}^K(\hat{t}/\hat{u}, \hat{s}) = \mathcal{P}^\pi(\hat{t}/\hat{u}, \hat{s})$ (see Ref.[17, 21]). Above we have written $\hat{s}, \hat{t}, \hat{u}$ to stress that these are quantities for a subprocess rather than for a full reaction. $\beta_M(\hat{s})$ and $\beta_R(\hat{s})$ are the phenomenological functions which role is to interpolate between meson and Reggeon exchange. Here, as in Ref.[17], we parametrize them as: $\beta_M(\hat{s}) = \exp(-(\hat{s} - 4m_K^2)/\Lambda_{int}^2)$, $\beta_R(\hat{s}) = 1 - \beta_M(\hat{s})$. The parameter Λ_{int} can be fitted to experimental data. From our general experience in hadronic physics we expect it to be about $\Lambda_{int} \sim 1 - 2$ GeV.

The form factors, $F(\hat{t}/\hat{u})$, correct for the off-shellness of the intermediate kaons in the middle of the diagrams shown in Fig. 3. In the following they are parameterized as

$$F_K(\hat{t}/\hat{u}) = \exp\left(\frac{\hat{t}/\hat{u} - m_K^2}{\Lambda_{off}^2}\right), \quad (2.8)$$

where the parameter Λ_{off} is not known in general but, in principle, could be fitted to the normalized experimental data. How to extract Λ_{off} will be discussed in the result section.

The absorptive corrections to the Born amplitude due to pp -interactions were taken into account in [17] as

$$\mathcal{M}^{pp\text{-rescatt.}} = \frac{i}{8\pi^2 s} \int d^2 \mathbf{k}_t A_{pp \rightarrow pp}^P(s, k_t^2) \mathcal{M}^{Born}(\mathbf{p}_{a,t}^* - \mathbf{p}_{1,t}, \mathbf{p}_{b,t}^* - \mathbf{p}_{2,t}), \quad (2.9)$$

where $p_a^* = p_a - k_t$, $p_b^* = p_b + k_t$ and k_t is the transverse momentum exchanged in the blob.

The formula presented so far do not include $\pi\pi, KK \rightarrow KK$ rescatterings. The pion-pion interaction at high energies was studied e.g. in Refs. [22, 23]. In full analogy to those works at the higher energies one can include the $\pi\pi, KK \rightarrow KK$ rescattering for our four-body reaction by replacing the normal (or reggeized) pion/kaon propagators (including vertex form factors).

The $KK \rightarrow KK$ subprocess amplitude for t and u diagrams in Fig. 3 is written in the high-energy approximation

$$\begin{aligned} \frac{F_K^2(\hat{t})}{\hat{t} - m_K^2} &\rightarrow \frac{i}{16\pi^2 \hat{s}} \int d^2 \kappa \frac{F_K^2(\hat{t}_1)}{\hat{t}_1 - m_K^2} M_{K^+K^- \rightarrow K^+K^-}(\hat{s}, \hat{t}_2), \\ \frac{F_K^2(\hat{u})}{\hat{u} - m_K^2} &\rightarrow \frac{i}{16\pi^2 \hat{s}} \int d^2 \kappa \frac{F_K^2(\hat{u}_1)}{\hat{u}_1 - m_K^2} M_{K^-K^+ \rightarrow K^-K^+}(\hat{s}, \hat{u}_2). \end{aligned} \quad (2.10)$$

Here the integration is over momentum in the loop (see [23]). The quantities \hat{t}_1 , \hat{u}_1 and \hat{t}_2 , \hat{u}_2 are four-momenta squared of the exchanged objects in the first and in the second step of the rescattering process. Other details are explained in [22].

The elastic amplitudes in the $KK \rightarrow KK$ subprocesses are written as

$$M_{KK \rightarrow KK}(\hat{s}, \hat{t}_2/\hat{u}_2) = \beta'_M(\hat{s}) A_{KK \rightarrow KK}^{V\text{-exch.}}(\hat{t}_2/\hat{u}_2) + \beta'_R(\hat{s}) A_{KK \rightarrow KK}^{Regge}(\hat{s}, \hat{t}_2/\hat{u}_2), \quad (2.11)$$

for vector meson ($V = \rho, \omega, \phi$) exchanges and $\beta'_M(\hat{s}) = \exp(-(\hat{s} - 4m_K^2)/\Delta\hat{s})$, $\beta'_R(\hat{s}) = 1 - \beta'_M(\hat{s})$, $\Delta\hat{s} = 9 \text{ GeV}^2$.

The Regge-type interaction which includes Pomeron and Reggeon (f_2 , a_2 , ρ and ω) exchanges applies at higher energies:

$$\begin{aligned} A_{K^+K^- \rightarrow K^+K^-}^{Regge}(\hat{s}, \hat{t}_2) &= \eta_i \hat{s} C_i^{KK} \left(\frac{\hat{s}}{\hat{s}_0} \right)^{\alpha_i(\hat{t}_2)-1} \exp\left(\frac{B_{KK}^i}{2} \hat{t}_2 \right), \\ A_{K^-K^+ \rightarrow K^-K^+}^{Regge}(\hat{s}, \hat{u}_2) &= \eta_i \hat{s} C_i^{KK} \left(\frac{\hat{s}}{\hat{s}_0} \right)^{\alpha_i(\hat{u}_2)-1} \exp\left(\frac{B_{KK}^i}{2} \hat{u}_2 \right), \end{aligned} \quad (2.12)$$

where the scale parameter \hat{s}_0 is taken as 1 GeV^2 and the C_i^{KK} coupling constants can be evaluated assuming Regge factorization $C_i^{KK} = (C_i^{KN})^2 / C_i^{NN}$ and are listed in Table I.

At low energies the Regge type of interactions is not realistic and rather $V = \rho, \omega, \phi$ meson exchanges must be taken into account:

$$\begin{aligned} A_{K^+K^- \rightarrow K^+K^-}^{V\text{-exch.}}(\hat{t}_2) &= g_{KKV} F_{KKV}(\hat{t}_2) \frac{(p_3^{*\mu} + p_3^\mu) P_{\mu\nu} (p_4^{*\nu} + p_4^\nu)}{\hat{t}_2 - m_V^2 + im_V \Gamma_V} g_{KKV} F_{KKV}(\hat{t}_2), \\ A_{K^-K^+ \rightarrow K^-K^+}^{V\text{-exch.}}(\hat{u}_2) &= g_{KKV} F_{KKV}(\hat{u}_2) \frac{(p_3^{*\mu} + p_3^\mu) P_{\mu\nu} (p_4^{*\nu} + p_4^\nu)}{\hat{u}_2 - m_V^2 + im_V \Gamma_V} g_{KKV} F_{KKV}(\hat{u}_2), \end{aligned} \quad (2.13)$$

where $P_{\mu\nu}(k) = -g_{\mu\nu} + k_\mu k_\nu / m_V^2$ and the KKV coupling constants g_{KKV} are given from SU(3) symmetry relations $2g_{KK\omega} = \sqrt{2}g_{KK\phi} = 2g_{KK\rho} = g_{\rho\pi\pi} = 6.04$ [24], where the value of $g_{\rho\pi\pi}$ is determined by the decay width of the ρ meson.

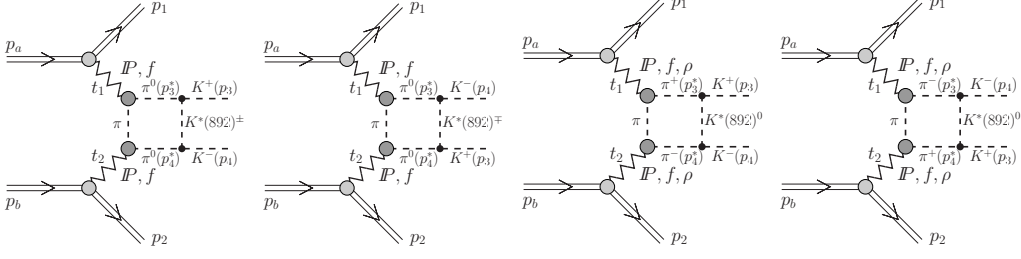


FIG. 4: The central diffractive mechanism of exclusive production of K^+K^- pairs via the $K^*(892)$ meson exchanges.

Again the $\pi\pi \rightarrow KK$ subprocess amplitude is written in the high-energy approximation as

$$\begin{aligned} \frac{F_\pi^2(\hat{t})}{\hat{t} - m_\pi^2} &\rightarrow \frac{i}{16\pi^2 \hat{s}} \int d^2\kappa \frac{F_\pi^2(\hat{t}_1)}{\hat{t}_1 - m_\pi^2} M_{\pi\pi \rightarrow K^+K^-}^{K^*-exch.}(\hat{t}_2), \\ \frac{F_\pi^2(\hat{u})}{\hat{u} - m_\pi^2} &\rightarrow \frac{i}{16\pi^2 \hat{s}} \int d^2\kappa \frac{F_\pi^2(\hat{u}_1)}{\hat{u}_1 - m_\pi^2} M_{\pi\pi \rightarrow K^-K^+}^{K^*-exch.}(\hat{u}_2), \end{aligned} \quad (2.14)$$

with

$$\begin{aligned} M_{\pi\pi \rightarrow K^+K^-}^{K^*-exch.}(\hat{t}_2) &= g_{\pi KK^*} F_{\pi KK^*}(\hat{t}_2) \frac{(p_3^{*\mu} + p_3^\mu) P_{\mu\nu}(p_4^{*\nu} + p_4^\nu)}{\hat{t}_2 - m_{K^*}^2 + im_{K^*}\Gamma_{K^*}} g_{\pi KK^*} F_{\pi KK^*}(\hat{t}_2), \\ M_{\pi\pi \rightarrow K^-K^+}^{K^*-exch.}(\hat{u}_2) &= g_{\pi KK^*} F_{\pi KK^*}(\hat{u}_2) \frac{(p_3^{*\mu} + p_4^\mu) P_{\mu\nu}(p_4^{*\nu} + p_3^\nu)}{\hat{u}_2 - m_{K^*}^2 + im_{K^*}\Gamma_{K^*}} g_{\pi KK^*} F_{\pi KK^*}(\hat{u}_2), \end{aligned} \quad (2.15)$$

where now $P_{\mu\nu}(k) = -g_{\mu\nu} + k_\mu k_\nu / m_{K^*}^2$ and we take $g_{\pi KK^*} = -\frac{1}{2} g_{\rho\pi\pi}$ [24].

The quantities $F(k^2)$ in Eqs (2.13, 2.15) describe couplings of extended ω and K^* mesons, respectively, and are parameterized in the exponential form:

$$F(k^2) = \exp\left(\frac{B_V}{4}(k^2 - m_V^2)\right). \quad (2.16)$$

Consistent with the definition of the coupling constant the form factors are normalized to unity when ω or K^* meson is on-mass-shell. We take $B_V = 4 \text{ GeV}^{-2}$.

The amplitudes given by formula (2.15) are corrected by the factors $(\hat{s}/\hat{s}_0)^{\alpha_{K^*}(k^2)-1}$ to reproduce the high-energy Regge dependence. We take K^* meson trajectory as $\alpha_{K^*}(k^2) = 0.25 + \alpha'_{K^*} k^2$, with $\alpha'_{K^*} = 0.83 \text{ GeV}^{-2}$ [21].

The cross section is obtained by integration over the four-body phase space, which is reduced to 8-dimensions and performed numerically

$$\sigma = \int \frac{1}{2s} |\overline{\mathcal{M}}|^2 (2\pi)^4 \delta^4(p_a + p_b - p_1 - p_2 - p_3 - p_4) \frac{d^3p_1}{(2\pi)^3 2E_1} \frac{d^3p_2}{(2\pi)^3 2E_2} \frac{d^3p_3}{(2\pi)^3 2E_3} \frac{d^3p_4}{(2\pi)^3 2E_4}. \quad (2.17)$$

The details how to conveniently reduce the number of kinematical integration variables are given e.g. in [6].

III. OTHER DIFFRACTIVE PROCESSES

Up to now we have discussed only central diffractive contribution to the $pp \rightarrow ppK^+K^-$ reaction. In general, there are also contributions with other diffractive processes shown in Fig.5, not e.valuated so far in the literature. It is straightforward to evaluate the new

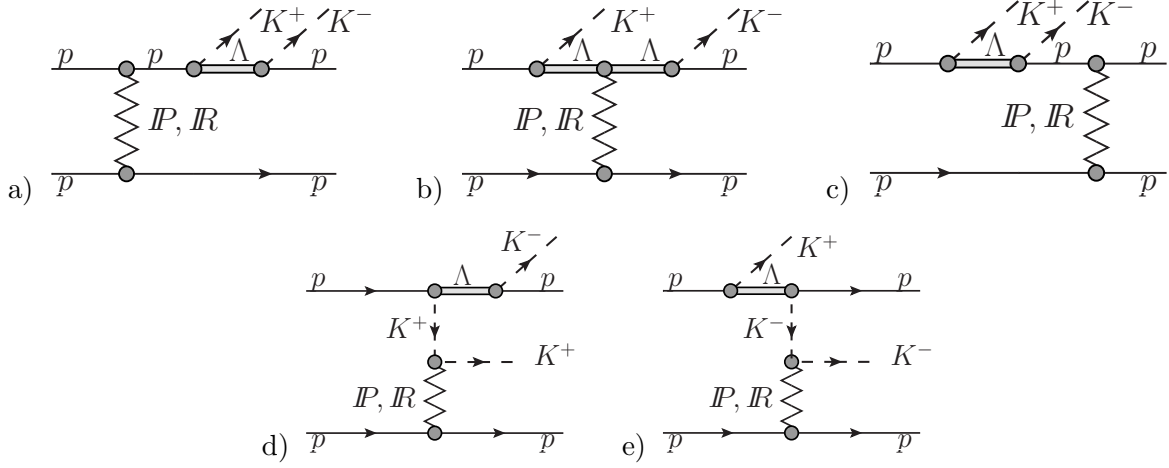


FIG. 5: Other diffractive contributions leading to the $pp \rightarrow ppK^+K^-$ channel.

diffractive contributions of diagrams a) - e) and the Born amplitudes are given below:

$$\begin{aligned} \mathcal{M}_{\lambda_a \lambda_b \rightarrow \lambda_1 \lambda_2}^{(a)} &= \bar{u}(p_1, \lambda_1) i\gamma_5 S_\Lambda(p_{1fl}^2) i\gamma_5 S_p(p_{1fp}^2) u(p_a, \lambda_a) g_{\Lambda KN}^2 F_p^2(p_{1fp}^2) F_\Lambda^2(p_{1fl}^2) \\ &\times i s C_{\mathbb{P}}^{NN} \left(\frac{s}{s_0} \right)^{\alpha_{\mathbb{P}}(t_2)-1} \exp \left(\frac{B_{\mathbb{P}}^{NN} t_2}{2} \right) \delta_{\lambda_2 \lambda_b}, \end{aligned} \quad (3.1)$$

$$\begin{aligned} \mathcal{M}_{\lambda_a \lambda_b \rightarrow \lambda_1 \lambda_2}^{(b)} &= \bar{u}(p_1, \lambda_1) i\gamma_5 S_\Lambda(p_{1fl}^2) S_\Lambda(p_{1il}^2) i\gamma_5 u(p_a, \lambda_a) g_{\Lambda KN}^2 F_\Lambda^2(p_{1il}^2) F_\Lambda^2(p_{1fl}^2) \\ &\times i s_{124} C_{\mathbb{P}}^{\Lambda N} \left(\frac{s_{124}}{s_0} \right)^{\alpha_{\mathbb{P}}(t_2)-1} \left(\frac{s_{134}}{s_{th}^{pKK}} \right)^{\alpha_\Lambda(p_{1il}^2)-1/2} \exp \left(\frac{B_{\mathbb{P}}^{\Lambda N} t_2}{2} \right) \delta_{\lambda_2 \lambda_b}, \end{aligned} \quad (3.2)$$

$$\begin{aligned} \mathcal{M}_{\lambda_a \lambda_b \rightarrow \lambda_1 \lambda_2}^{(c)} &= \bar{u}(p_1, \lambda_1) S_p(p_{1ip}^2) i\gamma_5 S_\Lambda(p_{1il}^2) i\gamma_5 u(p_a, \lambda_a) g_{\Lambda KN}^2 F_\Lambda^2(p_{1il}^2) F_p^2(p_{1il}^2) \\ &\times i s_{12} C_{\mathbb{P}}^{NN} \left(\frac{s_{12}}{s_0} \right)^{\alpha_{\mathbb{P}}(t_2)-1} \left(\frac{s_{14}}{s_{th}^{pK}} \right)^{\alpha_N(p_{1ip}^2)-1/2} \left(\frac{s_{34}}{s_{th}^{KK}} \right)^{\alpha_\Lambda(p_{1il}^2)-1/2} \exp \left(\frac{B_{\mathbb{P}}^{NN} t_2}{2} \right) \delta_{\lambda_2 \lambda_b}, \end{aligned} \quad (3.3)$$

$$\begin{aligned} \mathcal{M}_{\lambda_a \lambda_b \rightarrow \lambda_1 \lambda_2}^{(d)} &= \bar{u}(p_1, \lambda_1) i\gamma_5 S_\Lambda(p_{1fl}^2) i\gamma_5 u(p_a, \lambda_a) S_K(p_{1fk}^2) g_{\Lambda KN}^2 F_\Lambda^2(p_{1fl}^2) F_K^2(p_{1fk}^2) \\ &\times i s_{23} C_{\mathbb{P}}^{KN} \left(\frac{s_{23}}{s_0} \right)^{\alpha_{\mathbb{P}}(t_2)-1} \left(\frac{s_{134}}{s_{th}^{pKK}} \right)^{\alpha_K(p_{1fk}^2)-1} \exp \left(\frac{B_{\mathbb{P}}^{KN} t_2}{2} \right) \delta_{\lambda_2 \lambda_b}, \end{aligned} \quad (3.4)$$

$$\begin{aligned}
\mathcal{M}_{\lambda_a \lambda_b \rightarrow \lambda_1 \lambda_2}^{(e)} &= \bar{u}(p_1, \lambda_1) i\gamma_5 S_\Lambda(p_{1il}^2) i\gamma_5 u(p_a, \lambda_a) S_K(p_{1ik}^2) g_{\Lambda KN}^2 F_\Lambda^2(p_{1il}^2) F_K^2(p_{1ik}^2) \\
&\times i s_{24} C_P^{KN} \left(\frac{s_{24}}{s_0} \right)^{\alpha_P(t_2)-1} \left(\frac{s_{14}}{s_{th}^{pK}} \right)^{\alpha_K(p_{1ik}^2)-1} \left(\frac{s_{13}}{s_{th}^{pK}} \right)^{\alpha_\Lambda(p_{1il}^2)-1/2} \exp\left(\frac{B_P^{KN} t_2}{2} \right) \delta_{\lambda_2 \lambda_b},
\end{aligned} \tag{3.5}$$

where $s_0 = 1 \text{ GeV}^2$ and $s_{th}^{pK} = (m_N + m_K)^2$, $s_{th}^{pKK} = (m_N + 2m_K)^2$. In the above equations $u(p_i, \lambda_i)$, $\bar{u}(p_f, \lambda_f) = u^\dagger(p_f, \lambda_f) \gamma^0$ are the Dirac spinors (normalized as $\bar{u}(p)u(p) = 2m_N$) of the initial and outgoing protons with the four-momenta p and the helicities λ . Here $s_{ij} = (p_i + p_j)^2$, $s_{ijk} = (p_i + p_j + p_k)^2$ are squared invariant masses of the (i, j) and (i, j, k) systems. The four-momenta squared of the virtual particles are: $p_{1il,2il}^2 = (p_{a,b} - p_3)^2$, $p_{1fl,2fl}^2 = (p_{1,2} + p_4)^2 = s_{14,24}$, $p_{1ik,2ik}^2 = (p_{1il,2il} - p_{1,2})^2$, $p_{1fk,2fk}^2 = (p_{a,b} - p_{1il,2il})^2$, $p_{1ip,2ip}^2 = (p_{1il,2il} - p_4)^2$, $p_{1fp,2fp}^2 = (p_{1fl,2fl} + p_3)^2 = s_{134,234}$. While the four-momenta squared of transferred kaons and protons are < 0 , it is not the case for transferred Λ 's where $p_{1il,2il}^2 < m_\Lambda^2$. The propagators for the intermediate particles are respectively

$$\begin{aligned}
S_K(k^2) &= \frac{i}{k^2 - m_K^2}, \\
S_p(k^2) &= \frac{i(k_\nu \gamma^\nu + m_N)}{k^2 - m_N^2}, \\
S_\Lambda(k^2) &= \frac{i(k_\nu \gamma^\nu + m_\Lambda)}{k^2 - m_\Lambda^2}.
\end{aligned} \tag{3.6}$$

The form factors, $F_i(k^2)$, correct for the off-shellness of the virtual particles and are parameterised as

$$F_i(k^2) = \exp\left(\frac{-|k^2 - m_i^2|}{\Lambda_{off}^2} \right), \tag{3.7}$$

where the parameter $\Lambda_{off} = 1 \text{ GeV}$ is taken in practical calculations. In our calculation the ΛKN coupling constant is taken as $g_{\Lambda KN}^2 = 14$ [25].

The Regge parameters in diagram (b) in Fig.5 (see Eq.(3.2)) are not known precisely and are assumed to be $C_P^{\Lambda N} \approx C_P^{NN}$ (see Table I) and $B_P^{\Lambda N} \approx B_P^{NN} = 9 \text{ GeV}^{-2}$. To reproduce the high-energy Regge dependence the amplitudes given in Eqs (3.2 - 3.5) are corrected, e.g. the amplitude of (3.4) is multiplied by a factor $(s_{134}/s_{th}^{pKK})^{\alpha_K(p_{1fk}^2)-1}$. The parameters of the Regge trajectories used in the calculation are given as $\alpha_K(k^2) = 0.7(k^2 - m_K^2)$, $\alpha_p(k^2) = -0.3 + 0.9k^2$, $\alpha_\Lambda(k^2) = -0.6 + 0.9k^2$ for the kaon, proton and Λ exchanges, respectively.

Finally we consider the $\pi\pi \rightarrow KK$ rescattering mechanism shown in Fig.6 which is particularly important rather at lower energies, e.g. for experiment PANDA to be built at GSI Darmstadt. We write the Born amplitude according to Feynman rules as

$$\begin{aligned}
\mathcal{M}_{\lambda_a \lambda_b \rightarrow \lambda_1 \lambda_2}^{\pi\pi-KK}(\hat{t}, \hat{u}) &= \bar{u}(p_1, \lambda_1) i\gamma_5 u(p_a, \lambda_a) S_\pi(t_1) g_{\pi NN} F_{\pi NN}(t_1) F_{\pi K^* K}(t_1) \\
&\quad (M_{\pi\pi \rightarrow K^+ K^-}^{K^*-exch.}(\hat{t}) + M_{\pi\pi \rightarrow K^- K^+}^{K^*-exch.}(\hat{u})) \\
&\quad \bar{u}(p_2, \lambda_2) i\gamma_5 u(p_b, \lambda_b) S_\pi(t_2) g_{\pi NN} F_{\pi NN}(t_2) F_{\pi K^* K}(t_2),
\end{aligned} \tag{3.8}$$

where $g_{\pi NN}^2/4\pi = 13.5$ value is taken and the $M_{\pi\pi \rightarrow KK}^{K^*-exch.}$ amplitudes are given by Eq.(2.15).

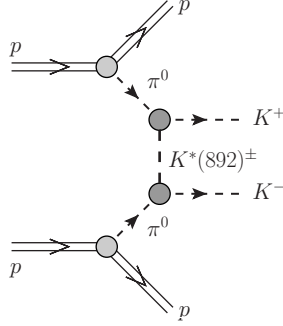


FIG. 6: The $\pi\pi \rightarrow KK$ subprocess leading to the $pp \rightarrow ppK^+K^-$ reaction.

IV. RESULTS

Now we wish to show results and predictions for existing and future experiments. We start with DPE mechanism which dominates at midrapidities. In Fig. 7 we show the two-kaon invariant mass distribution at the center-of-mass energy of the CERN ISR $\sqrt{s} = 62$ GeV [26] (this is the highest energy at which normalized experimental data exist). In this calculation the experimental cuts on the rapidity of both kaons and on longitudinal momentum fractions (Feynman- x , $x_F = 2p_{\parallel}/\sqrt{s}$) of both outgoing protons are included. The experimental data show some small peaks above our flat model continuum. They correspond to the K^+K^- resonances (e.g. $f_2(1270)$, $f'_2(1525)$) which are not included explicitly in our calculation. In the present analysis we are interested mostly what happens above the region $M_{KK} > 2-3$ GeV (see right panel). The results depend on the value of the nonperturbative, a priori unknown parameter of the form factor responsible for off-shell effects (see Eq. (2.8)). Our model with $\Lambda_{off}^2 = 2$ GeV² cut-off parameter fitted to the data provides an educated extrapolation to the unmeasured region. We compare results without (dotted lines) and with absorption corrections including the KK -rescattering effect (solid line). At the χ_{c0} mass the KK -rescattering leads to an enhancement of the cross section compared to the calculation without KK -rescattering. Below we shall use also this background predictions when analyzing the signal (χ_{c0}) to background ratio.

In Fig. 8 we show differential distributions for the $pp \rightarrow ppK^+K^-$ reaction at $\sqrt{s} = 7$ TeV without (dotted line) and with (solid line) the absorptive corrections. In most distributions the shape is almost unchanged. The only exception is the distribution in proton transverse momentum where we predict a damping of the cross section at small proton p_t and an enhancement of the cross section at large proton p_t .

In Fig. 9 we show differential distributions in kaon rapidity $y_K = y_3 = y_4$ for the $pp \rightarrow ppK^+K^-$ reaction at $\sqrt{s} = 0.5, 1.96, 7$ TeV without (upper lines) and with (bottom lines) absorption effects. The integrated cross section slowly rises with incident energy. The reader is asked to notice that the energy dependence of the cross section at $y_K \approx 0$ is reversed by the absorption effects which are stronger at higher energies. In our calculation we include both Pomeron and Reggeon exchanges. The camel-like shape of the distributions is due to the interference of the components in the amplitude. In Fig.10 we show the distribution in $y_K = y_3 = y_4$ for all ingredients included (thick solid line) and when only Pomeron exchanges are included (solid line), separately for Pomeron-Reggeon (Reggeon-Pomeron) exchanges which peaks at backward (forward) kaon rapidities and in the case when only

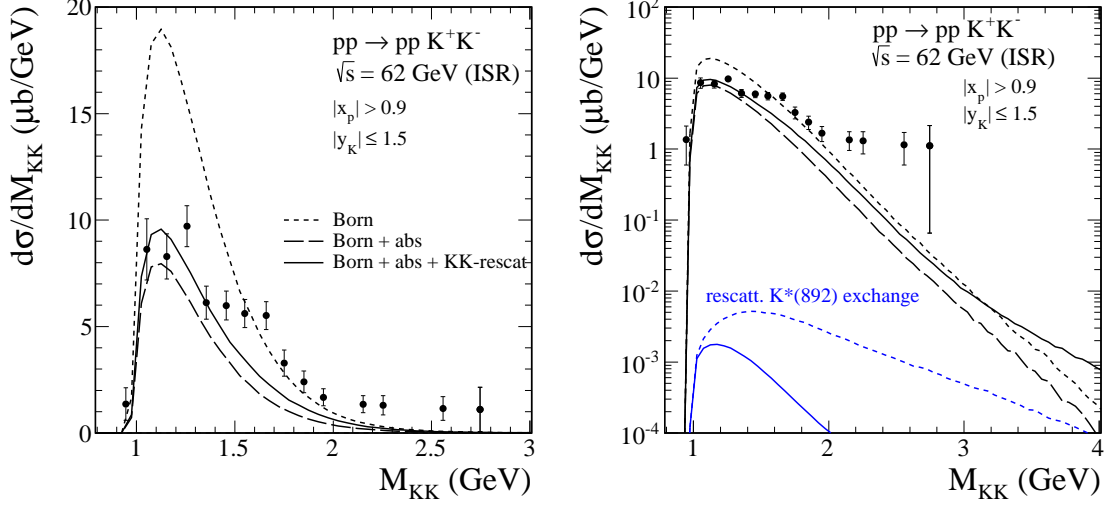


FIG. 7: Differential cross section $d\sigma/dM_{KK}$ for the $pp \rightarrow pp K^+ K^-$ reaction at $\sqrt{s} = 62$ GeV with experimental cuts relevant for the CERN ISR experimental data from Ref. [26]. Right panel shows the same in logarithmic scale. Results without (dotted line) and with (solid line) absorption effects are shown. Here $\Lambda_{off}^2 = 2 \text{ GeV}^2$ and $\Lambda_{int} = 2 \text{ GeV}$.

Reggeon exchanges are included (dashed line).

In Fig.11 we show distributions in the two-dimensional (y_3, y_4) space at $\sqrt{s} = 0.5, 1.96, 7$ TeV for the central diffractive contribution. The cross section grows with \sqrt{s} . At high energies the kaons are emitted preferentially in the same hemispheres, i.e. $y_3, y_4 > 0$ or $y_3, y_4 < 0$. In this calculation the cut-off parameter $\Lambda_{off}^2 = 2 \text{ GeV}^2$.

In Fig.12 we show distributions in the $(p_{t,K}, M_{KK})$ space at $\sqrt{s} = 0.5, 7$ TeV for the central diffractive contribution. As expected we observe strong correlation between the two variables.

Now we wish to compare differential distributions of kaon from the χ_{c0} decay with those for the continuum kaons. The corresponding amplitude for exclusive central diffractive χ_{c0} meson production was obtained within the k_t -factorization approach including virtualities of active gluons [9] and the corresponding cross section is calculated with the help of unintegrated gluon distribution functions (UGDFs) known from the literature. In the first step we calculate the two-dimensional distribution $d\sigma(y, p_t)/dy dp_t$, where y is rapidity and p_t is the transverse momentum of χ_{c0} . The decay of $\chi_{c0} \rightarrow K^+ K^-$ is included then in a simple Monte Carlo program assuming isotropic decay of the scalar χ_{c0} meson in its rest frame. The kinematical variables of kaons are transformed to the overall center-of-mass frame where extra cuts are imposed. Including the simple cuts we construct several differential distributions in different kinematical variables.

In Fig. 13 we show two-kaon invariant mass distribution for the central diffractive KK continuum and the contribution from the decay of the χ_{c0} meson (see the peak at $M_{KK} \simeq 3.4$ GeV) and the contribution from the decay of the ϕ meson. The cross section for exclusive production of the ϕ meson has been calculated within a pQCD k_t -factorization approach in Ref.[27]. In these figures the resonant $\mathcal{R} = \phi, \chi_{c0}$ distributions was parameterized in the

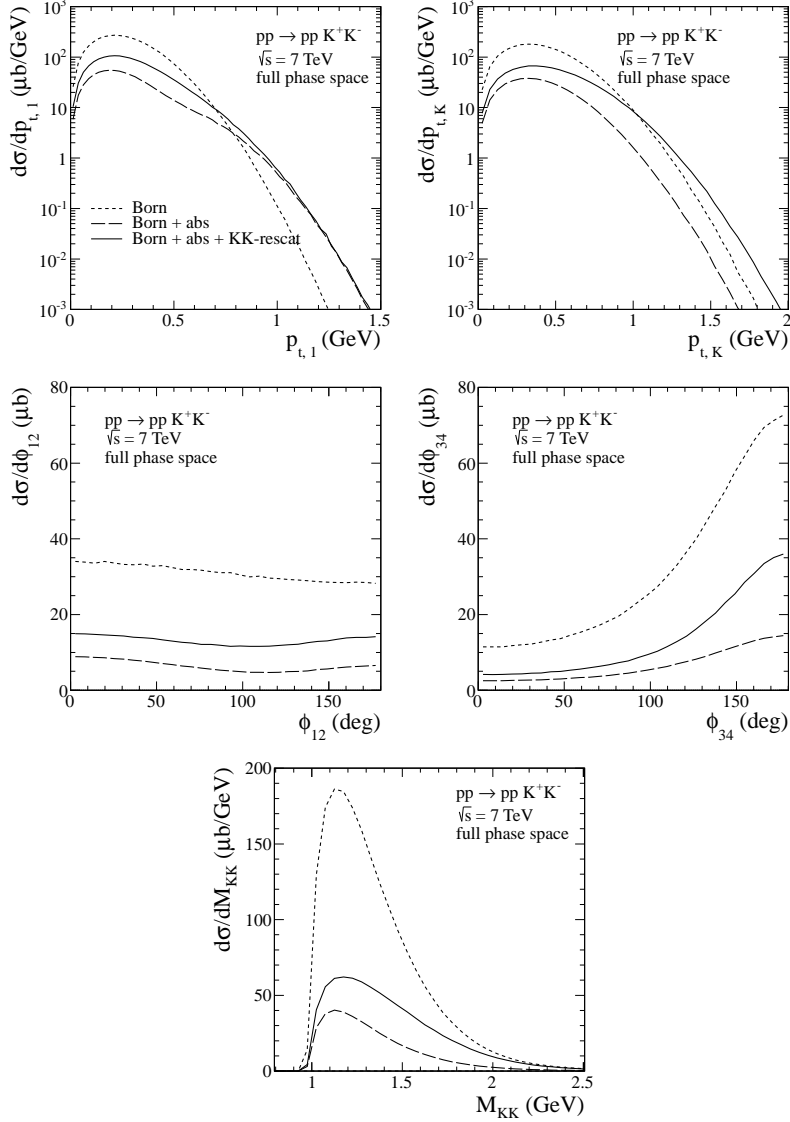


FIG. 8: Differential cross sections for the $pp \rightarrow pp K^+ K^-$ reaction at $\sqrt{s} = 7$ TeV without (dotted line) and with (solid line) the absorption effects. These calculations were done with the cut-off parameter $\Lambda_{off}^2 = 2 \text{ GeV}^2$ and $\Lambda_{int} = 2 \text{ GeV}$.

Breit-Wigner form:

$$\frac{d\sigma}{dM_{KK}} = \mathcal{B}(\mathcal{R} \rightarrow K^+ K^-) \sigma_{pp \rightarrow pp \mathcal{R}} 2M_{KK} \frac{1}{\pi} \frac{M_{KK} \Gamma_{\mathcal{R}}}{(M_{KK}^2 - m_{\mathcal{R}}^2)^2 + M_{KK}^2 \Gamma_{\mathcal{R}}^2}, \quad (4.1)$$

with parameters according to particle data book [16]. In the calculation of the χ_{c0} distributions we use GRV94 NLO [28] and GJR08 NLO [29] collinear gluon distributions. The cross sections for the ϕ and χ_{c0} production and for the background include absorption effects. While the upper row shows the cross section integrated over the full phase space at different energies, the lower rows show results including the relevant kaon pseudorapidity restrictions $-1 < \eta_{K^+}, \eta_{K^-} < 1$ (RHIC and Tevatron) and $-2.5 < \eta_{K^+}, \eta_{K^-} < 2.5$ (LHC). Shown are only purely theoretical predictions. In reality the situation is, however, somewhat worse

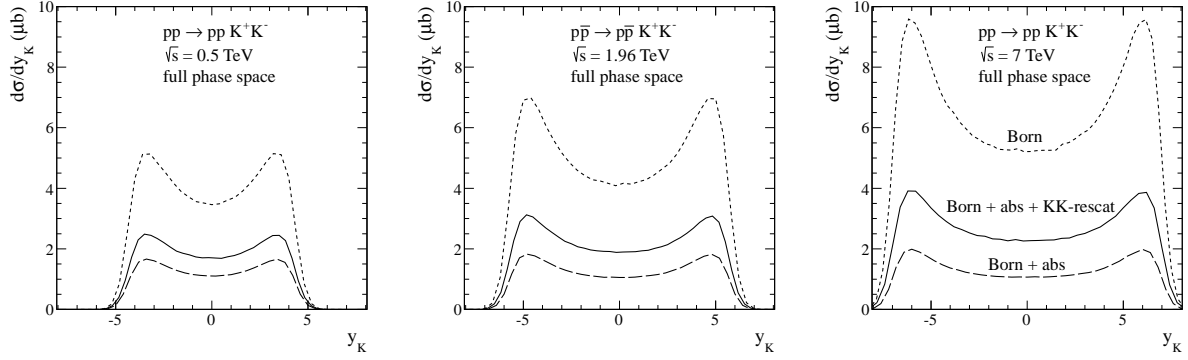


FIG. 9: Differential cross section $d\sigma/dy_K$ for the $pp \rightarrow pp K^+ K^-$ reaction at $\sqrt{s} = 0.5, 1.96, 7$ TeV with $\Lambda_{off}^2 = 2 \text{ GeV}^2$. The results without (upper lines) and with (bottom lines) absorption effects due to pp -interaction and KK -rescattering are shown too.

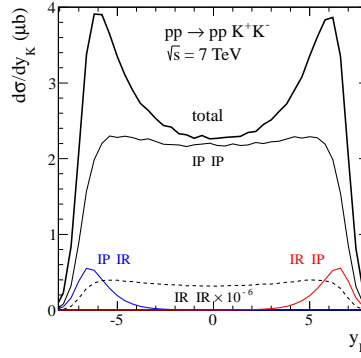


FIG. 10: Differential cross section $d\sigma/dy_K$ for the $pp \rightarrow pp K^+ K^-$ reaction at $\sqrt{s} = 7$ TeV with $\Lambda_{off}^2 = 2 \text{ GeV}^2$. The different lines corresponds to the situation when all and only some components in the amplitude are included. The details are explained in the main text.

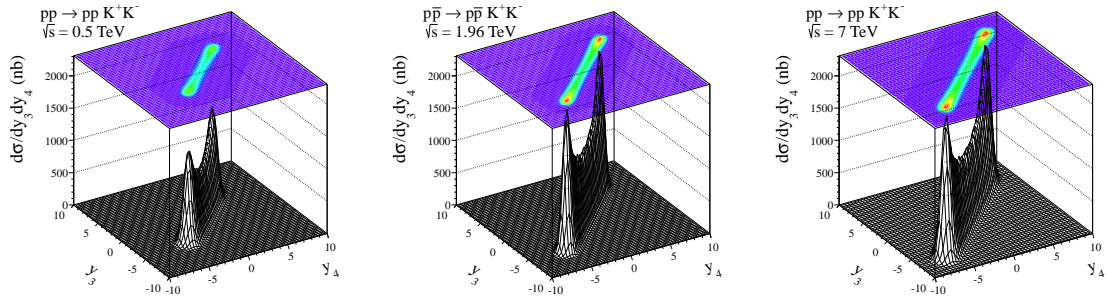


FIG. 11: Differential cross section in (y_3, y_4) for the central diffractive contribution for three incident energies $\sqrt{s} = 0.5, 1.96, 7$ TeV. The absorption effects were included here.

as both protons and, in particular, kaon pairs are measured with a certain precision which

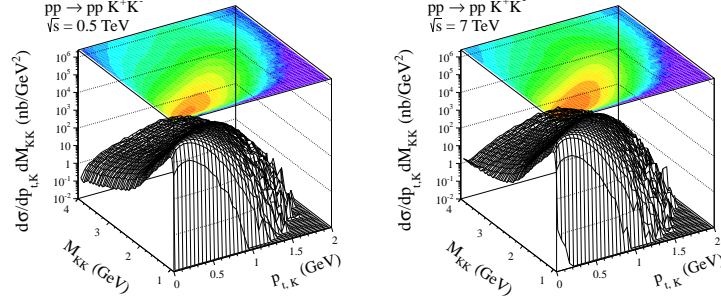


FIG. 12: Differential cross section in $(p_{t,K}, M_{KK})$ for the central diffractive contribution for two incident energies $\sqrt{s} = 0.5, 7$ TeV. The absorption effects were included here.

TABLE II: Integrated cross sections in μb (with absorption corrections) for exclusive K^+K^- production at different energies. In this calculations we have taken into account the relevant limitations in the pion pseudorapidities $|\eta_K| < 1$ at RHIC and Tevatron, $|\eta_K| < 2.5$ at LHC.

\sqrt{s} (TeV)	full phase space	with cuts on η_K
0.5	18.47	1.21
1.96	27.96	1.37
7	41.14	7.38

leads to an extra smearing in M_{KK} . While the smearing is negligible for the background, it

leads to a modification of the Breit-Wigner peak for the χ_{c0} meson¹. The results with more modern GJR UGDF are smaller by about a factor of 2-3 than those for somewhat older GRV UGDF.

In Fig. 14 we show distributions in kaon transverse momenta. The kaons from the χ_{c0} decay are placed at slightly larger $p_{t,K}$. This can be therefore used to get rid of the bulk of the continuum by imposing an extra cut on the kaon transverse momenta. It is not the case for the kaons from the ϕ decay which are placed at lower $p_{t,K}$.

In Table II we have collected numerical values of the integrated cross sections for exclusive production of K^+K^- at different energies. In Table III we have collected in addition numerical values of the integrated cross sections (see $\sigma_{pp \rightarrow pp\chi_{c0}}$ in Eq. (4.1)) for exclusive χ_{c0} production for some selected UGDFs at different energies.

In Fig.15 we present rapidity distribution of K^+ (left panel) and rapidity distribution of K^- (right panel) including only diagrams shown in Fig.5. The contribution for individual diagrams a) - e) are also shown. In the discussed here new mechanism not only protons but also kaons are produced dominantly in very forward or very background directions forming a large size gap in rapidity. Please note a very limited range of rapidities shown in the figure.

¹ An additional experimental resolution not included here can be taken into account by an extra convolution of the Breit-Wigner shape with an additional Gaussian function.

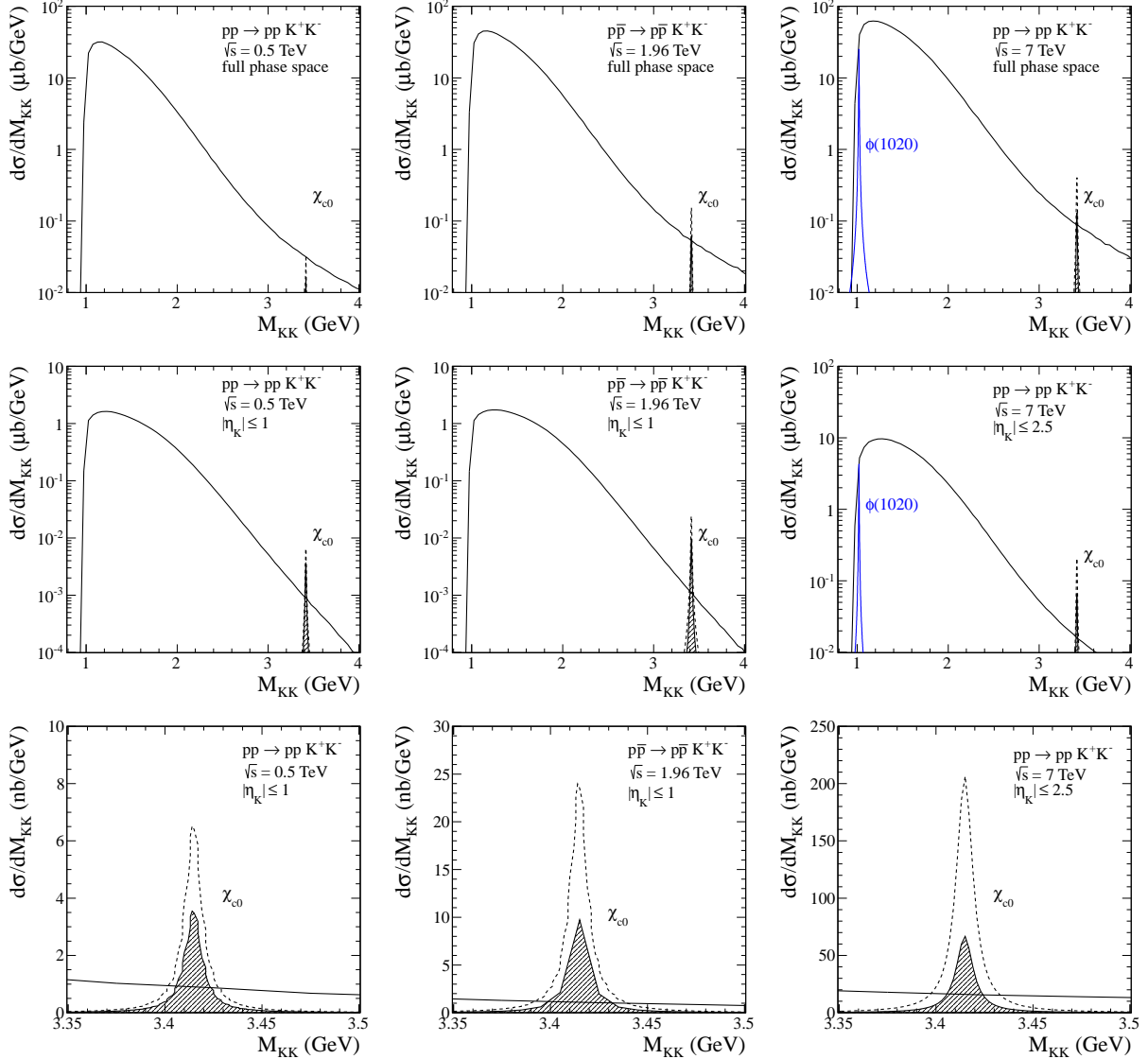


FIG. 13: The K^+K^- invariant mass distribution at $\sqrt{s} = 0.5, 1.96, 7$ TeV integrated over the full phase space (upper row) and with the detector limitations in pion pseudorapidities (lower rows). The solid lines present the KK continuum with the cut-off parameters $\Lambda_{off}^2 = 2 \text{ GeV}^2$. The χ_{c0} contribution is calculated with the GRV94 NLO (dotted lines) and GJR08 NLO (filled areas) collinear gluon distributions. The cross section for ϕ contribution at $\sqrt{s} = 7$ TeV is calculated as in [27]. The absorption effects were included in the calculations. Clear χ_{c0} signal with relatively small background can be observed.

The reggeization leads to an extra damping of the cross section. The cross section is much smaller than that for the DPE mechanism discussed above. It is particularly interesting that the distributions for K^+ and K^- have slightly different shape.

Finally, the general situation at high energies is sketched in Fig.16. The discussed in this paper central diffractive (DD) contribution lays along the diagonal $y_3 = y_4$ and the classical DPE is placed in the center $y_3 \approx y_4$. While the contribution from diagrams in Fig.5 is predicted at $y_3, y_4 \sim y_{beam}$ or $y_3, y_4 \sim y_{target}$, the $\pi\pi \rightarrow KK$ contribution (see Fig.6) is

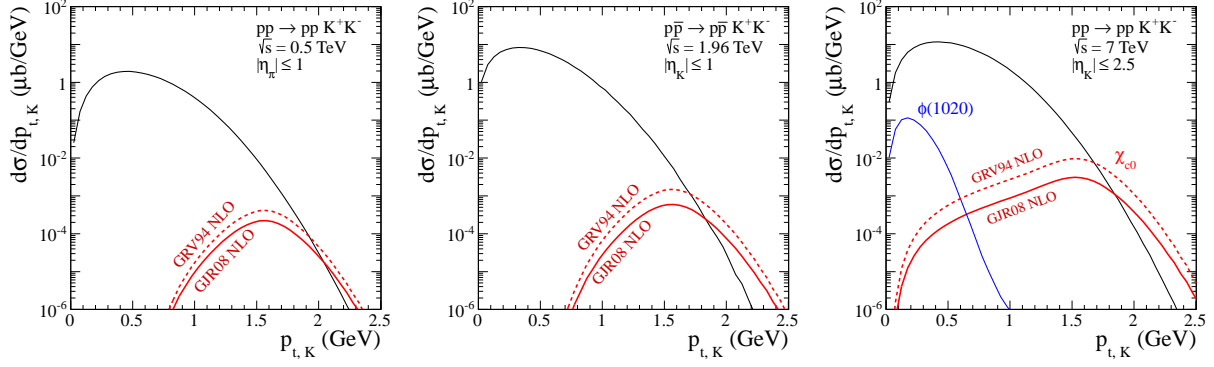


FIG. 14: Differential cross section $d\sigma/dp_{t,K}$ at $\sqrt{s} = 0.5, 1.96, 7$ TeV with cuts on the kaon pseudorapidities. The diffractive background was calculated with the cut-off parameter $\Lambda_{off}^2 = 2 \text{ GeV}^2$. Results for the kaons from the decay of the χ_{c0} meson including the K^+K^- branching ratio, for the GRV94 NLO (upper lines) and GJR08 NLO (bottom lines) UGDFs, are shown. In the right panel ϕ meson contribution is shown in addition. The absorption effects were included here.

TABLE III: Integrated cross sections in nb (with absorption corrections) for exclusive χ_{c0} production at different energies with the GRV94 NLO and GJR08 NLO collinear gluon distributions. In these calculations we have taken into account the relevant limitations in the kaon pseudorapidities $|\eta_K| < 1$ at RHIC and Tevatron, $|\eta_K| < 2.5$ at LHC and lower cut on both kaon transverse momenta $|p_{t,K}| > 1.5 \text{ GeV}$.

\sqrt{s} (TeV)	full phase space		with cuts on η_K		with cuts on η_K and $p_{t,K}$	
	GRV	GJR	GRV	GJR	GRV	GJR
0.5	82.9	44.0	17.3	9.4	5.7	3.1
1.96	406.3	165.1	63.7	25.9	20.7	8.3
7	1076.7	347.7	548.6	177.1	114.5	36.6
14	1566.3	449.2	735.0	210.9	152.1	43.1

predicted at ($y_3 \sim y_{beam}$ and $y_4 \sim y_{target}$) or ($y_3 \sim y_{target}$ and $y_4 \sim y_{beam}$), i.e. well separated from the central diffractive contribution. The separation in the (y_3, y_4) space can be used to separate the two contributions experimentally.

V. CONCLUSIONS

In the present paper we have calculated several differential observables for the exclusive $pp \rightarrow pp K^+ K^-$ and $p\bar{p} \rightarrow p\bar{p} K^+ K^-$ reactions. The full amplitude of central diffractive process was calculated in a simple model with parameters adjusted to low energy data. The energy dependence of the amplitudes of the KN subsystems was parametrized in the Regge form which describes total and elastic cross section for the KN scattering. This parametrization includes both leading Pomeron trajectory as well as subleading Reggeon exchanges. We have predicted large cross sections for RHIC, Tevatron and LHC which

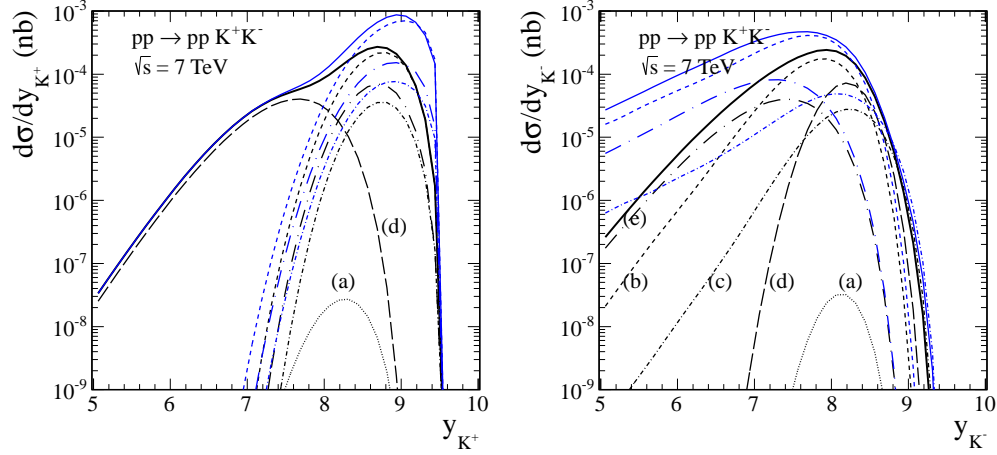


FIG. 15: Differential cross sections $d\sigma/dy_{K^+}$ (left panel) and $d\sigma/dy_{K^-}$ (right panel) for the $pp \rightarrow ppK^+K^-$ reaction at $\sqrt{s} = 7$ TeV. The solid line represents the coherent sum of all amplitudes. The dotted, dashed, dash-dotted, long-dashed, long-dash-dotted lines correspond to contributions from a) - e) diagrams in Fig.5. The upper (blue online) lines correspond to contributions without reggeization of Λ propagator in diagrams b), c), e).

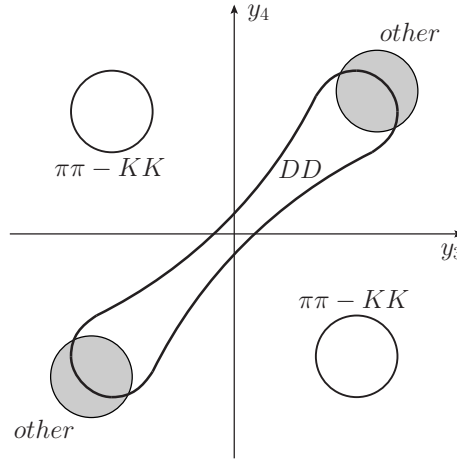


FIG. 16: A schematic localization of different mechanisms for the $pp \rightarrow ppK^+K^-$ reaction at high energies.

allows to hope that presented by us distributions will be measured.

We have calculated also contributions of several diagrams where kaons are emitted from the proton lines. These mechanisms contribute at forward and backward regions and do not disturb in the observation of the central DPE component.

It was realized recently at the Tevatron that the measurement of exclusive production of χ_c via decay in the $J/\psi + \gamma$ channel cannot provide production cross sections for different species of χ_c . In this decay channel the contributions of χ_c mesons with different spins are similar and experimental resolution is not sufficient to distinguish them.

In the present paper we have analyzed a possibility to measure the exclusive production of χ_{c0} meson in the proton-(anti)proton collisions at the LHC, Tevatron and RHIC via

$\chi_{c0} \rightarrow K^+ K^-$ decay channel. We have performed detailed studies of several differential distributions and demonstrated how to impose extra cuts in order to improve the signal-to-background ratio. We have shown that relevant measurements at RHIC, Tevatron and LHC are possible. Since the cross section for exclusive χ_{c0} production is much larger than for $\chi_{c(1,2)}$ and the branching fraction to the KK channel for χ_{c0} is larger than that for χ_{c2} (χ_{c1} does not decay into two kaons) the two-kaon channel should provide an useful information about the χ_{c0} exclusive production.

-
- [1] A. Dzyuba *et al.*, Phys. Lett. **B668** (2008) 315.
 - [2] Ju-Jun Xie and Colin Wilkin, Phys. Rev. **C82** (2010) 025210.
 - [3] M.G. Albrow, T.D. Coughlin and J.R. Forshaw, Prog. Part. Nucl. Phys. **65** (2010) 149.
 - [4] A. Szczurek and P. Lebiedowicz, Nucl. Phys. **A826** (2009) 101.
 - [5] P. Lebiedowicz, A. Szczurek and R. Kamiński, Phys. Lett. **B680** (2009) 459.
 - [6] P. Lebiedowicz and A. Szczurek, Phys. Rev. **D81** (2010) 036003.
 - [7] P. Lebiedowicz and A. Szczurek, Phys. Rev. **D83** (2011) 076002.
 - [8] R. Staszewski, P. Lebiedowicz, M. Trzebiński, J. Chwastowski and A. Szczurek, Acta Phys. Polon. **B42** (2011) 1861.
 - [9] R.S. Pasechnik, A. Szczurek and O.V. Teryaev, Phys. Rev. **D78** (2008) 014007.
 - [10] R.S. Pasechnik, A. Szczurek and O.V. Teryaev, Phys. Lett. **B680** (2009) 62.
 - [11] R.S. Pasechnik, A. Szczurek and O.V. Teryaev, Phys. Rev. **D81** (2010) 034024.
 - [12] L.A. Harland-Lang, V.A. Khoze, M.G. Ryskin and W.J. Stirling, Eur. Phys. J. **C65** (2010) 433.
 - [13] L.A. Harland-Lang, V.A. Khoze, M.G. Ryskin and W.J. Stirling, Eur. Phys. J. **C71** (2011) 1545.
 - [14] C. Amsler and F.E. Close, Phys. Rev. **D53** (1996) 295.
 - [15] T. Aaltonen *et al.* [CDF Collaboration], Phys. Rev. Lett. **102** (2009) 242001.
 - [16] K. Nakamura *et al.* [Particle Data Group], J. Phys. **G37** (2010) 075021.
 - [17] P. Lebiedowicz, R. Pasechnik and A. Szczurek, Phys. Lett. **B701** (2011) 434.
 - [18] M. Ablikim *et al.* [BESIII Collaboration], arXiv:hep-ex/1103.2661.
 - [19] A. Donnachie and P.V. Landshoff, Phys. Lett. **B296** (1992) 227.
 - [20] A. Eide *et al.*, Nucl. Phys. **B60** (1973) 173; I. Ambats *et al.*, Phys. Rev. **D9** (1974) 1179; C.W. Akerlof *et al.*, Phys. Rev. **D14** (1976) 2864; D.S. Ayres *et al.*, Phys. Rev. **D15** (1977) 3105.
 - [21] M. Guidal, J.M. Laget and M. Vanderhaeghen, Nucl. Phys. **A627** (1997) 645; Byung Geel Yu, Tae Keun Choi and W. Kim, Phys. Rev. **C83** (2011) 025208.
 - [22] A. Szczurek, N.N. Nikolaev and J. Speth, Phys. Rev. **C66** (2002) 055206.
 - [23] A. Szczurek and J. Speth, Nucl. Phys. **A728** (2003) 182.
 - [24] O. Krehl, R. Rapp and J. Speth, Phys. Lett. **B390** (1997) 23.
 - [25] J.M. Laget, Phys. Lett. **B259** (1991) 23.
 - [26] A. Breakstone *et al.* [ABCDHW Collaboration], Z. Phys. **C42** (1989) 387.
 - [27] A. Cisek, W. Schäfer and A. Szczurek, Phys. Lett. **B690** (2010) 168.
 - [28] M. Glück, E. Reya and A. Vogt, Z. Phys. **C67** (1995) 433.
 - [29] M. Glück, D. Jimenez-Delgado and E. Reya, Eur. Phys. J. **C53** (2008) 355; M. Glück, D. Jimenez-Delgado, E. Reya and C. Schuck, Phys. Lett. **B664** (2008) 133.